Investigation of specific heat in ultrathin two-dimensional superconducting Pb

T. D. Nguyen,[1] A. Frydman,[2,1,*] and O. Bourgeois[1,3,†]
[1]*Institut Néel, CNRS, BP 166, 38042 Grenoble Cedex 9, France*
[2]*The Department of Physics, Bar Ilan University, Ramat Gan 52900, Israel*
[3]*Université Grenoble Alpes, Inst NEEL, F-38042 Grenoble, France*

(Received 28 July 2019; revised manuscript received 16 December 2019; published 13 January 2020)

Superconductivity in two dimensions is nontrivial. One way to achieve global superconductivity is via the Berezinskii-Kosterlitz-Thouless (BKT) transition due to proliferation of vortex-antivortex pairs. This transition is expected to have a clear signature on the specific heat. The singularity at the transition temperature T_{BKT} is predicted to be immeasurable, and a broad nonuniversal peak is expected at $T > T_{\mathrm{BKT}}$. Up to date, this has not been observed in two-dimensional superconductors; this work is then dedicated to investigate c_p signatures in the limit of ultrathin 2d superconductors. We use a unique highly sensitive technique to measure the specific heat of quench condensed ultrathin Pb films. We find that thick films exhibit a specific heat jump at T_C that is consistent with BCS theory. As the film thickness is reduced below the superconducting coherence length and the systems enter the 2D limit, the specific heat reveals BKT-like behavior in what can appear as to be a continuous BCS-BKT crossover as a function of film thickness. However, a number of problems arise with this interpretation. We discuss the experimental results and the possible significance of various scenarios involving BKT physics.

DOI: 10.1103/PhysRevB.101.014509

I. INTRODUCTION

Within the 2D XY model, a second-order phase transition cannot take place due to the lack of long-range phase coherence and the dominance of phase fluctuations (Goldstone modes). Nevertheless, Berezinskii and Kosterlitz-Thouless (BKT) [1,2] showed that a low-temperature quasiordered phase of bound vortex pairs exists leading to an infinite order phase transition from bound vortex-antivortex pairs at low temperatures to unpaired vortices above the BKT critical temperature T_{BKT}. From the thermodynamic point of view, BKT theory predicts that the specific heat c_p is characterized by an immeasurable essential singularity at $T = T_{\mathrm{BKT}}$ and a nonuniversal peak at $T > T_{\mathrm{BKT}}$ associated with the liberation of entropy due to the unbounding of vortex-antivortex pairs [3]. Work on this transition led to the 2016 Nobel prize in Physics being awarded to Kosterlitz and Thouless.

A paradigmatic system in which the BKT transition may be expected is a 2D superconducting film. Evidence for the BKT physics have been reported in transport measurements via analysis of the *I-V* characteristics or by studying the perpendicular magnetoresistance curves [4–7]. However, up to date, there have been no experimental thermodynamic signatures of this transition, especially concerning 2D superconducting films. This requires a highly sensitive thermal experiment that is able to resolve the specific heat of ultrathin films in the limit of 2D superconductivity [8–10].

Here we report on specific heat c_p measurements performed on ultrathin superconducting films. We utilize a unique experimental setup based on a suspended silicone membrane substrate that enables us to measure c_p of quench condensed Pb films with thicknesses ranging from 1.2 to 56 nm. We show that the thicker films can be well described by the BCS theory for strongly coupled superconductors. In particular, they exhibit a specific heat jump at the critical temperature T_C characteristic of the second-order phase transition. Much thinner films, on the other hand, do not possess a measurable jump at T_C but are rather characterized by a broad c_p peak at $T > T_C$ indicating the presence of an excess of entropy. Qualitatively, these results are qualitatively consistent with the thermodynamic signatures expected from a thickness driven BCS-BKT crossover. There are, however, some quantitative problems with this interpretation as described below.

II. EXPERIMENTAL

A. Sample preparation and experimental setup

The samples used in this work were sets of ultrathin Pb films having different thickness obtained by the quench condensation technique [11–15], i.e., sequential evaporations of ultrathin films on a cryogenically cooled substrate without thermal cycling to room temperature or exposing the film to the atmosphere [see Fig. 1(a)]. This allows *in situ* sequential depositions under UHV conditions and simultaneous transport and thermal measurements on a single sample. Due to its unique advantages, this experimental method allows the study of the thermodynamic properties of the superconducting transition in ultrathin layers as a function of thickness.

Such quench-condensed thin layers are known to undergo an insulator-to-superconductor transition as a function of thickness. It was theoretically claimed by Anderson [16] that *s*-wave superconductivity is surprisingly robust against weak

*aviad.frydman@gmail.com
†olivier.bourgeois@neel.cnrs.fr

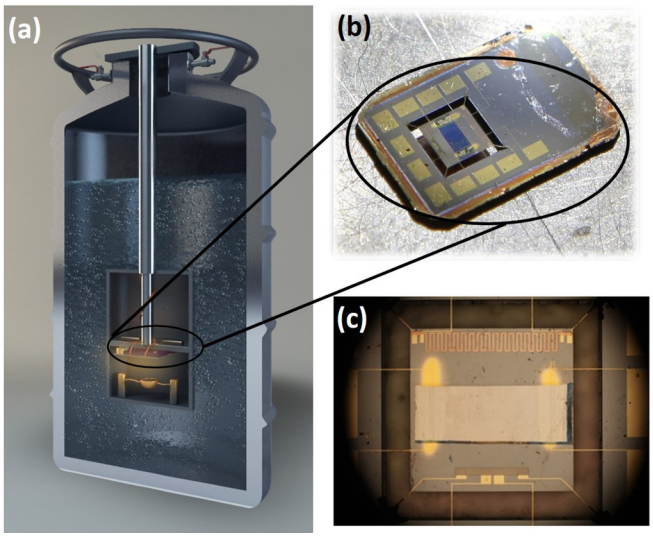

FIG. 1. (a) The quench condensation setup consists of evaporation baskets used for growing sequential continuous Pb layers, the substrate being held at cryogenic temperatures and in UHV conditions. [(b) and (c)] The suspended membrane acting as the thermal cell contains a copper meander, used as a heater, and a niobium nitride strip, used as a thermometer. These are lithographically fabricated close to the two edges of the active thermal sensor. The quench-condensed films are evaporated through a shadow mask which, together with the measurement leads, defines its geometry.

disorder of nonmagnetic impurities. Experimentally, however, it was found that T_C reduces with increasing disorder. It has been shown that for thin quench-condensed superconducting films the reason for this reduction is the suppression of the density of states due to electronic interactions which become more important as the disorder is increased. Nevertheless, BCS physics is maintained even for relatively highly disordered films as manifested by the constant ratio of $2\Delta/T_C$ [17].

The Pb thin films were evaporated layer by layer onto a calorimetric membrane sensor. The quench condensation system consists of three thermal evaporators to deposit different materials on the Si membrane-based calorimeter at cryogenic temperatures. For obtaining continuous ultrathin films, a thin Sb adhesion layer of about 2.5 nm thick is evaporated onto the cryocooled substrate prior to the deposition of the first Pb layer. The first evaporated Pb layers is subnanometer thick, electrically insulating, having a heat capacity too low to be measured. We got a measurable C_p signal for a layer of 1.2 nm for which the superconducting critical temperature is $T_{C_{\rm res}} = 2.12$ K. Details of the different layers are listed in Table I.

The layers are quench condensed on a uniquely designed 5-μm-thick Si membrane based calorimeter suspended by 12 arms. The thermal sensor consists of a NbN thermometer 70 nm thick and a heater made of Cu (100 nm thick) installed on each side of the membrane to free space for the evaporated samples [18]. All the microfabrication steps of the calorimeter are done using optical lithography. The electrical connections to all transducing elements on the membrane are obtained by a superconducting layer of (70 nm) NbTi/(20 nm) Au deposited on the suspending arms. In order to ensure a good electrical connection to very thin films (few angstroms), we evaporate (5 nm)WTi/(100 nm)Au on the contacts through a shadow

TABLE I. Experimental data extracted from the heat capacity measurements of the 22 evaporations (refereed to by sample number). For each evaporation of Pb, we give the mass, the heat capacity C_p at 7.5 K, the thickness t, the heat capacity jump ΔC_p at T_c, the specific heat jump Δc_p at T_c, the resistance per square R_{sq}, and the T_c and the entropy of the superconducting electron S_{7K} at 7 K extracted from the heat capacity measurements.

deposition number	mass (μg)	C_p (nJ K^{-1})	t (nm)	ΔC_p (nJ K^{-1})	Δc_p (mJ g^{-1} K^{-1})	R_{sq} (Ohm)	T_c (K)	S_{7K} (mJ K^{-1})
1	0.04891	0.31433	1.22431	NA	NA	6436	2.15	1.08
2	0.05789	0.5115	1.44923	NA	NA	3716	2.88	0.815
3	0.05953	0.5715	1.49018	NA	NA	3311	3.04	0.878
4	0.06242	0.58425	1.56269	NA	NA	2738	3.29	0.967
5	0.0678	0.633	1.69733	NA	NA	2316	3.53	1.07
6	0.07198	0.68175	1.80188	NA	NA	2046	3.75	0.914
7	0.07988	0.7575	1.99973	NA	NA	1636	4.02	1.03
8	0.08701	0.79275	2.1783	NA	NA	1304	4.24	0.997
9	0.09815	0.9	2.45709	NA	NA	1068	4.50	0.87
10	0.10853	1.035	2.71694	NA	NA	866	4.71	0.983
11	0.12348	1.125	3.09115	NA	NA	680	4.93	0.826
12	0.14963	1.3275	3.74573	NA	NA	478	5.23	0.785
13	0.17192	1.635	4.30375	NA	NA	323.2	5.46	0.967
14	0.205	1.8675	5.13177	NA	NA	225	5.72	0.851
15	0.22791	2.11592	5.70546	NA	NA	148.4	5.93	0.876
16	0.25914	2.4058	6.48711	NA	NA	91.1	6.22	0.606
17	0.2892	2.6849	7.23968	NA	NA	44.6	6.42	0.35
18	0.32558	3.0227	8.15055	0.1324	0.40665	28.3	6.66	0.251
19	0.49785	4.62197	12.4629	0.21696	0.4358	15.9	6.82	0.133
20	0.89413	8.30106	22.38336	0.3562	0.39838	8.6	6.90	0.122
21	1.70387	15.81861	42.65404	0.53438	0.31363	4.6	6.97	0.0365
22	2.23188	20.72058	55.87194	0.7678	0.34402	3.5	7.00	0.0146

mask to make the profile smooth. Using this setup we were able to measure simultaneously the resistance per square R_{sq} using four probe techniques and the heat capacity C_p.

The calorimeter is wire-bonded to a sample holder that is mounted on the quench-condensation system, a vacuum chamber immersed in liquid helium and cooled down to $T = 2$ K. The sequential evaporations of Pb layers are carried out through a mechanical mask defining a window of 1.14 mm × 3.09 mm on the membrane, while temperature on the sample holder is regulated at 10 K during the material growth.

B. Heat capacity measurement technique

The heat capacity measurement was performed using the ac-calorimetry technique [19,20], in which an ac current with frequency f is applied to the heater, leading to the oscillation of the Si membrane temperature at the second harmonic $2f$ with amplitude of δT_{ac} [8,9]. Measuring the temperature oscillation enables us to extract the heat capacity using the equation

$$C_p = \frac{P_{ac}}{4\pi f \delta T_{ac}} \tag{1}$$

with P_{ac} is the Joule heating power dissipated in the heater.

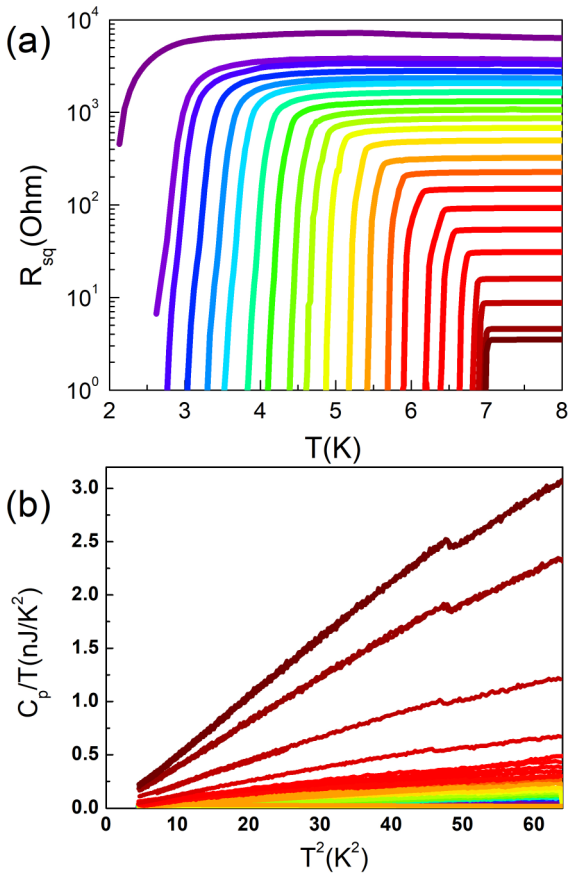

FIG. 2. (a) Resistance per square R_{sq} vs temperature for the 22 sequential quench condensed lead films. Purple is for thin films and red-brown for thick films. This color code is maintained throughout the paper. (b) Heat capacity of the films (same color code) in form of C_p/T vs T^2 highlighting the cubic behavior above 7.2 K.

Prior to the first deposition, the heat capacity of the bare calorimeter (without sample) is measured in the temperature range from 2 to 8 K. This was taken as a background for all consecutive layers. For each layer (including the Sb wetting layer), we simultaneously performed $R(T)$ and $C_p(T)$ measurements in the range 2 to 8 K. For each stage, we extracted the specific heat by dividing the heat capacity by the layer mass: $c_p^i = C_{Pb}^i/m^i$. The mass of the deposited Pb m^i was determined by a quartz microbalance integrated in the quench-condensation system and compared to the expected values from the superconducting transition temperature $T_{C_{res}}^i$ based on previous publication [14].

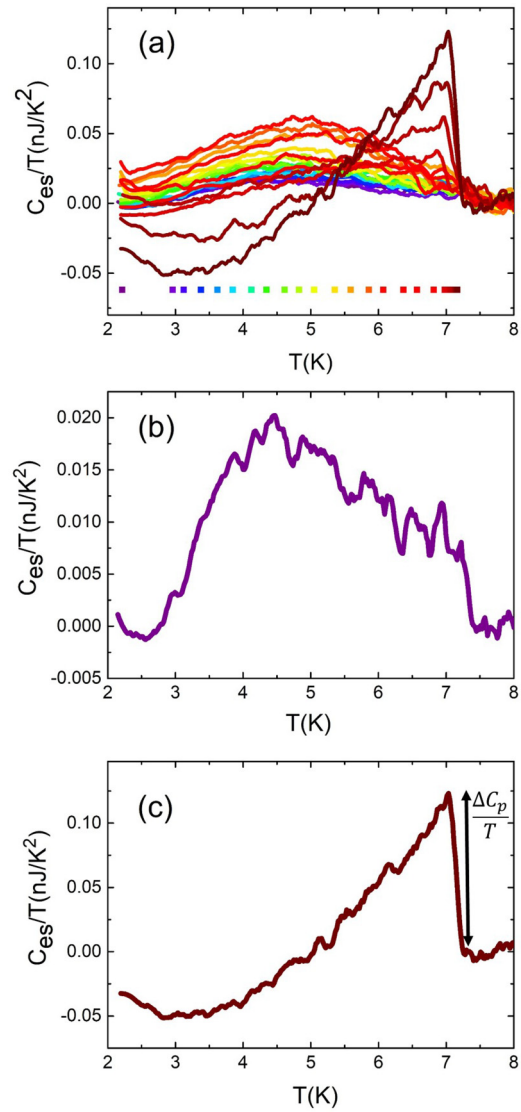

FIG. 3. (a) Superconducting electronic heat capacity C_{es} of the films normalized to temperature as extracted from the data presented in Fig. 2 along with an identical color code. The squares mark the $T_{C_{res}}$ of each layer extracted from the RT curves of Fig. 2(a). The curves for the 1.2-nm and 55-nm-thick films are shown in (b) and (c), respectively. In (c), the arrow represents the heat capacity jump normalized to temperature.

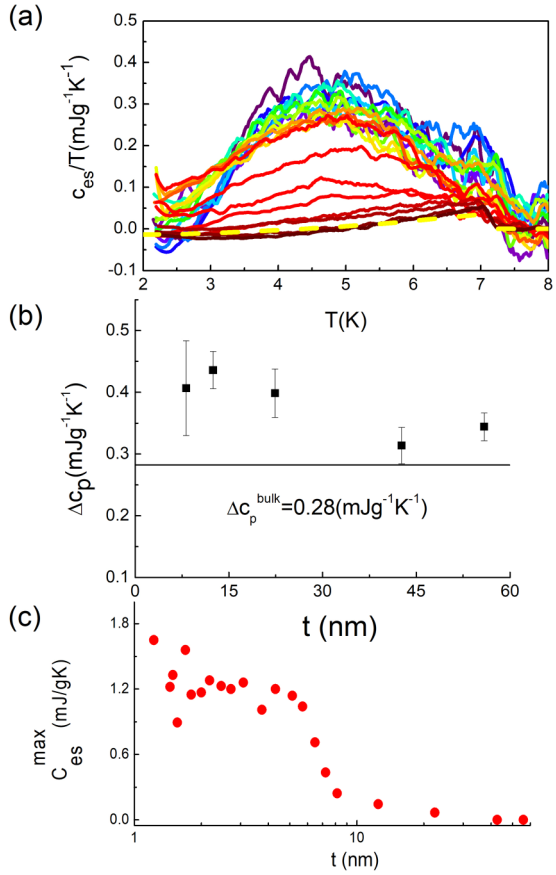

FIG. 4. (a) Specific heat of electrons in the superconducting state c_{es} normalized to temperature vs T. The squares mark the $T_{C_{res}}$ of each layer extracted from the RT curves of Fig. 2(a). The yellow dashed line is a fit to BCS expectation. (b) The amplitude of the specific heat jump at T_C, Δc_p, as a function of thickness. (c) The maximum value of the specific heat, normalized to the specific heat of layer 22, as a function of thickness.

III. RESULTS

Figure 2(a) shows resistance versus temperature curves of a set of quench condensed Pb films with thicknesses ranging between 1.2 and 56 nm. From these measurements, we extracted the critical temperature $T_{C_{res}}$, defined as the temperature at which resistance dropped to 10% of its value at $T = 10$ K. $T_{C_{res}}$ increased monotonically with increasing thickness of the lead layer, t. Our thinnest film ($t = 1.22$ nm) exhibited $T_{C_{res}} = 2.15$ K while films with $t \geqslant 12$ nm had critical temperatures close to that of bulk Pb $T_{C_{bulk}} = 7.2$ K. These values are in agreement with previous studies on ultrathin quench condensed Pb films [14]. The heat capacity (C_p) measurements of the same films are shown in Fig. 2(b), they are obtained after subtraction of the membrane heat capacity (Si, heater, and thermometer).

The heat capacity of a metallic sample is expected to follow the well known form:

$$\frac{C_n}{T} = \gamma + \beta T^2 \tag{2}$$

where γ and β stand for the electron and phonon heat capacities coefficients, respectively. For this reason, the data are plotted as C_p/T versus T^2 resulting in a linear normal-state curve above T_C. The heat capacity increased with film thickness and at high enough thickness, $t \geqslant 8$ nm (stage 18 and above), we observed a C_p jump associated with the superconductor second-order phase transition. The temperature position of the jump is consistent with the slight decrease of $T_{C_{res}}$ with decreasing thickness in this regime [see Fig. 2(a)]. The amplitude of the jump, ΔC_p, defined as $\Delta C_p = (C_p - C_n)_{T=T_c}$, decreases with decreasing thickness until for $t \leqslant 9$ nm the jump becomes immeasurable, smaller than the noise. We note, however, that even for the thickest film (layer 22, $t = 55.9$ nm) the ratio between the jump amplitude and the normal state heat capacity C_p at T_C, $\Delta C_p/C_n(T_c) = 0.0445$ is much smaller than the expected BCS value of 1.4 obtained for bulk Pb, for instance [21]. Like for Nb [22] and Al [23], this indicates that the heat capacity of amorphous Pb films is largely dominated by the phonon contribution.

In order to focus only on the heat capacity contribution of electrons in the superconducting state C_{es} we subtract the normal state C_p, extracted from the linear slope in T^2 above $T_{C_{bulk}} = 7.2$ K, from each respective curve of Fig. 2(b) thus obtaining $C_{es} = C_p - C_n$ (see Appendix 1). C_{es} for the different layers are shown in Fig. 3(a). C_{es} versus T for the thinnest and thickest films are shown in panels (b) and (c) of Fig. 3, respectively. The curves for the thickest films are consistent with results obtained on bulk Pb samples [21].

Obtaining the specific heat, c_p, from the measured heat capacity C_p is achieved by dividing the curve of each layer in Fig. 3(a) by its mass: $c_p^i = C_p^i/m^i$. The electronic specific heat c_{es} (defined as $c_{es}^i = C_{es}^i/m^i$) normalized to temperature versus T curves for all layers are shown in Fig. 4. It is seen that the specific heat jump amplitude for the thicker films is very close to that observed in bulk Pb samples, $\Delta c_p = \Delta C_p/m \sim 0.28$ mJ g^{-1} K^{-1} as shown in Fig. 4(b) (see Appendix A). This is in stark contrast to results obtained on granular Pb films [10] for which Δc_p was found to be larger than the bulk value by up to a factor of eight.

As the film is thinned, Δc_p becomes immeasurable and an excess specific heat peak emerges with a temperature region that extends up to $T_{C_{bulk}} = 7.2$ K. These results are qualitatively consistent with a crossover from 3D BCS physics, characterized by $T_c = 7.2$ K, and to 2D BKT physics with $T_{BKT} \approx 2$ K for the thinnest films, while the intermediate layers show a mixture of both.

IV. DISCUSSION

The representation shown in Fig. 4 highlights the importance of the broad peaks which become more significant as the thickness of the layer is reduced. The magnitude of this peak (c_{es}^{max}), increases sharply for $t \leqslant 10$ nm and saturates for $t \leqslant 5$ nm as depicted in Fig. 4(c). This saturation of the specific heat peak amplitude for thicknesses below 5 nm is consistent with the superconducting film becoming 2D. The superconducting dirty limit coherence length, ξ', of the amorphous Pb is given by $\sqrt{\xi_0 l}$, where ξ_0 is the clean limit coherence length (80 nm for Pb) and l is the mean free path which for our samples is 0.3 nm [24]. This yields $\xi' = 4.9$ nm. Hence, the excess

specific heat bump reaches its full amplitude as the film thickness becomes comparable to the coherence length.

However, there are a number of problems with the above interpretation. (1) The amplitude of the specific heat peak at $T > T_{\mathrm{BKT}}$ is much larger than what could be naively expected if each vortex degrees of freedom contributes $2k_B$ to C_p [3]. Assuming a single vortex per coherence length, ξ', the measured peak amplitude is close to two orders of magnitude larger than the expected value.

(2) A point to consider is related to the sample dimensionality. The electronic heat capacity includes contributions both from quasiparticles and from vortices. For quasiparticle the system has to be treated as 3D, and the specific heat should be obtained by dividing the heat capacity by the layer thickness (or by the mass). The vortices, on the other hand, should organize in a 2D plane once $t < \xi'$, and hence the vortex contribution to heat capacity is not expected to change with growing thickness. In this respect, it is interesting to compare Fig. 3(a), which is representative of a 2D treatment, and Fig. 4(a), which highlights 3D physics. One could expect that the heat capacity peak amplitude, $C_{\mathrm{es}}^{\mathrm{max}}$ in Fig. 3(a) would not change with thickness for thin films. It should be noted, however, that ultrathin superconducting films have been shown to be characterized by "emergent electronic granularity," i.e., superconducting puddles embedded in an insulating matrix [25–29]. These puddles may have different sizes and thus a spread of critical temperatures [30]. This may be the reason why the specific heat in the thinnest films does not posses a jump at T_C similar to the one observed in granular Pb samples where each grain is large enough to sustain bulk superconductivity [10]. Thin enough layers may actually not achieve full coverage of the substrate, both morphologically and electronically. Increasing the thickness of film may increase the area of superconducting regions leading to increase the vortex contribution to heat capacity even in the 2D limit.

(3) The resistance versus temperature curves show one sharp drop at T_c without a second transition. For the above interpretation one has to assume that the sharp resistance drop occurs at T_{BKT} rather than T_c which remains the bulk value for any film thickness. This is not consistent with previous tunneling measurements that showed that the for ultrathin quench-condensed superconducting films the energy gap, Δ, reduces with decreasing thickness [17]. In this experiment, it was found that BCS physics is maintained even for very thin films as manifested by the constant ratio of $2\Delta/T_C$.

V. CONCLUSIONS

In summary, we have successfully performed specific heat measurements on Pb films as thin as 1.2 nm having a mass as small as few tens of nanograms. We have shown that for the thicker films the specific heat jump is well described by the BCS model for strongly coupled superconductivity. For the thinner films, a broad peak in c_p is observed without any measurable jump at the resistive critical temperature. These are qualitatively consistent with the BKT predictions in the limit of ultrathin uniform superconducting films, however, as noted above, there are still a number of problems with this interpretation and other scenarios should also be considered. Since the details of the specific heat versus temperature curves are predicted to be nonuniversal and are system dependent, we are not able to compare our results to a quantitative model. Clearly, further theoretical work is needed to shed light on the issues raised in this paper.

ACKNOWLEDGMENTS

We are grateful for useful discussions with M. Holzmann, N. Trivedi, and M. Randera and for the support from the technical pole of Institut NEEL especially from E. André, T. Crozes, A. Gérardin, G. Moiroux, and J.-L. Mocellin. We acknowledge support from the Laboratoire d'excellence LANEF in Grenoble (ANR-10-LABX-51-01). A.F. acknowledges support from the NSF-BSF Grant No. 2017677 and the Israel Science Foundation, Grant No. 783/17.

APPENDIX A: SPECIFIC HEAT COMPONENTS

The total specific heat has at least two components a phonon and an electron contributions. For this work, only matters the electronic contribution in the superconducting state to the specific heat. It is usually calculated using the following equation:

$$c_{\mathrm{es}} = c_s - c_n, \tag{A1}$$

where c_s is the specific heat measured at zero field, which shows superconducting transition in the present case, $c_s = c_p^i$; c_n is the specific heat in the normal state measured at magnetic field greater than the critical field. In our experiment, the critical field is expected to be much bigger than the limitation of our setup (the maximum available magnetic field is of 2 T) [31]. In this case, we used an alternative strategy to estimate the electronic contribution. First, we fitted the specific heat of the normal state, above T_c for stage 22 with a function: $c_n^{22} = \gamma T + \beta T^3 + \zeta T^5$, and then extrapolated to temperature below T_c to find c_n^{22} in the whole temperature range of the measurement from 2 to 8 K. This c_n^{22} was then used to estimate the electronic specific heat for all stages since the specific heat at normal state of all 22 stages are nearly overlapped. And so, the electronic specific heat for each stage is estimated by the following equation:

$$c_{\mathrm{es}}^i = c_p^i - c_n^{22}. \tag{A2}$$

APPENDIX B: FITTING THE ELECTRONIC SPECIFIC HEAT WITH THE α MODE

It has been reported in number of works [21,32] that bulk Pb is a strong-coupling superconductor, for which the BCS model does not fit the electronic specific heat very well. H. Padamsee and coworkers have developed an extended model based on BCS theory, the so called "α model" in 1973 [32]. In this model, they introduced a free or adjustable parameter $\alpha \equiv \Delta(0)/k_B T_c$, which becomes a means of scaling the BCS gap:

$$\Delta(T) = (\alpha/\alpha_{\mathrm{BCS}})\Delta_{\mathrm{BCS}}(T) \tag{B1}$$

with α_{BCS} is the weak-coupling value of the gap ratio 1.764. With this free parameter α, the entropy of the superconducting

electron becomes

$$S_{es}(t)/\gamma T_c = -(3\alpha/\pi^2)\int_0^\infty dx[f_x ln f_x + (1-f_x)ln(1-f_x)], \tag{B2}$$

where $f_x = [\exp(\alpha t^{-1}(x^2+\delta^2)^{1/2})+1]^{-1}$, $t = T/T_c$ and $\delta = \Delta(T)/\Delta(0)$ is the reduced gap. The specific heat of the superconducting electron is then calculated by the following equation:

$$C_{es}/\gamma T_c = t(d/dt)(S_{es}/\gamma T_c). \tag{B3}$$

In order to fit the specific heat of the superconducting electron obtained at stage 22 (c_{es}^{22}), we firstly used MATHLAB to calculate numerically the specific heat of the superconducting electrons based on the α model. This calculation gives us c_{es}^{α}. Since the c_{es}^{22} is obtained by removal from the c_p^{22} the extrapolation of the normal state, which contains also the electronic contribution (γT). Therefore, to obtain the fit to our data, we have to subtract from the calculated specific heat a specific heat contribution coming from the normal electrons (γT). It is also known that the γ coefficient of strong-coupling superconductors like Pb is not a constant but temperature dependent [21,32–34]. Thus we have fitted our data (c_{es}^{22}) with $c_{es}^{\alpha} - \gamma(T)T$. The fit is shown in Fig. 5.

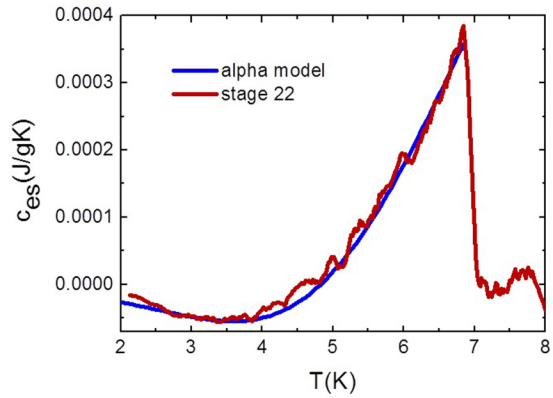

FIG. 5. Fitting the electronic specific heat obtained from the last stage with α model.

We found that the fit is in good agreement when we set $\alpha = 2.7$, and the γ is a temperature dependent function $\gamma(T) = 8\times10^{-7}\times T^2 + 10^{-5}$ (J g^{-1} K^{-2}), in good agreement with what has been observed for bulk Pb in the past [32].

[1] V. L. Berezinskii, Zh. Eksp. Teor. Fiz. **61**, 1144 (1971) [Sov. Phys. JETP **34**, 610 (1972)].
[2] J. M. Kosterlitz and D. J. Thouless, J. Phys. C **6**, 1181 (1973).
[3] P. M. Chaikin and T. C. Lubensky, *Principles of Condensed Matter Physics* (Cambridge University Press, Cambridge, 1995), Vol. 550.
[4] P. Minnhagen, Rev. Mod. Phys. **59**, 1001 (1987).
[5] K. Epstein, A. M. Goldman, and A. M. Kadin, Phys. Rev. Lett. **47**, 534 (1981).
[6] S. A. Wolf, D. U. Gubser, W. W. Fuller, J. C. Garland, and R. S. Newrock, Phys. Rev. Lett. **47**, 1071 (1981).
[7] A. F. Hebard and A. T. Fiory, Phys. Rev. Lett. **50**, 1603 (1983).
[8] O. Bourgeois, S. E. Skipetrov, F. Ong, and J. Chaussy, Phys. Rev. Lett. **94**, 057007 (2005).
[9] S. Poran, M. Molina-Ruiz, A. Gérardin, A. Frydman, and O. Bourgeois, Rev. Sci. Instrum. **85**, 053903 (2014).
[10] S. Poran, T. Nguyen-Duc, A. Auerbach, N. Dupuis, A. Frydman, and O. Bourgeois, Nat. Commun. **8**, 14464 (2017).
[11] M. Strongin, R. S. Thompson, O. F. Kammerer, and J. E. Crow, Phys. Rev. B **1**, 1078 (1970).
[12] R. C. Dynes, J. P. Garno, and J. M. Rowell, Phys. Rev. Lett. **40**, 479 (1978).
[13] R. C. Dynes, A. E. White, J. M. Graybeal, and J. P. Garno, Phys. Rev. Lett. **57**, 2195 (1986).
[14] D. B. Haviland, Y. Liu, and A. M. Goldman, Phys. Rev. Lett. **62**, 2180 (1989).
[15] O. Bourgeois, A. Frydman, and R. C. Dynes, Phys. Rev. Lett. **88**, 186403 (2002).
[16] P. W. Anderson, Phys. Rev. **109**, 1492 (1958).
[17] J. M. Valles, Jr., R. C. Dynes, and J. P. Garno, Phys. Rev. B **40**, 6680 (1989).
[18] T. Nguyen, A. Tavakoli, S. Triqueneaux, R. Swami, A. Ruhtinas, J. Gradel, P. Garcia-Campos, K. Hasselbach, A. Frydman, B. Piot, M. Gibert, E. Collin, and O. Bourgeois, J. Low Temp. Phys. **197**, 348 (2019).
[19] P. F. Sullivan and G. Seidel, Phys. Rev. **173**, 679 (1968).
[20] F. Fominaya, T. Fournier, P. Gandit, and J. Chaussy, Rev. Sci. Instrum. **68**, 4191 (1997).
[21] C. A. Shiffman, J. F. Cochran, and M. Garber, J. Phys. Chem. Solids **24**, 1369 (1963).
[22] A. Brown, M. W. Zemansky, and H. A. Boorse, Phys. Rev. **92**, 52 (1953).
[23] D. L. Martin, Proc. Phys. Soc. **78**, 1489 (1961).
[24] O. Bourgeois, A. Frydman, and R. C. Dynes, Phys. Rev. B **68**, 092509 (2003).
[25] D. Kowal and Z. Ovadyahu, Solid State Commun. **90**, 783 (1994); Physica C **468**, 322 (2008).
[26] A. Ghosal, M. Randeria, and N. Trivedi, Phys. Rev. Lett. **81**, 3940 (1998).
[27] A. Ghosal, M. Randeria, and N. Trivedi, Phys. Rev. B. **65**, 014501 (2001).
[28] M. V. Feigel'man, L. B. Ioffe, V. E. Kravtsov, and E. A. Yuzbashyan, Phys. Rev. Lett. **98**, 027001 (2007).
[29] K. Bouadim, Y. Loh, M. Randeria, and N. Trivedi, Nat. Phys. **7**, 884 (2011).
[30] J. Biscaras, N. Bergeal, S. Hurand, C. Feuillet-Palma, A. Rastogi, R. C. Budhani, M. Grilli, S. Caprara, and J. Lesueur, Nat. Mater. **12**, 542 (2013).
[31] C. K. Schiller and H. Bulow, J. Appl. Phys. **40**, 4179 (1969).
[32] H. Padamsee, J. E. Neighbor, and C. A. Shiffman, J. Low Temp. Phys. **12**, 387 (1973).
[33] G. Grimvall, Solid State Commun. **7**, 213 (1969).
[34] G. Grimvall, J. Phys. Chem. Solids **29**, 1221 (1968).